2D Materials

PAPER • OPEN ACCESS

Epitaxial growth of *γ*-InSe and *α*, *β*, and *γ*-In_2Se_3 on *ε*-GaSe

IOP Publishing 2D Mater. 5 (2018) 035026 https://doi.org/10.1088/2053-1583/aac479

2D Materials

PAPER

Epitaxial growth of γ-InSe and α, β, and γ-In_2Se_3 on ε-GaSe

CrossMark

RECEIVED
26 April 2018

ACCEPTED FOR PUBLICATION
14 May 2018

PUBLISHED
1 June 2018

Nilanthy Balakrishnan[1], Elisabeth D Steer[2], Emily F Smith[2], Zakhar R Kudrynskyi[1], Zakhar D Kovalyuk[3], Laurence Eaves[1], Amalia Patanè[1] and Peter H Beton[1]

[1] School of Physics and Astronomy, University of Nottingham, Nottingham NG7 2RD, United Kingdom
[2] Nanoscale and Microscale Research Centre, The University of Nottingham, Nottingham NG7 2RD, United Kingdom
[3] Institute for Problems of Materials Science, The National Academy of Sciences of Ukraine, Chernivtsi Branch, Chernivtsi 58001, Ukraine

E-mail: nilanthy.balakrishnan@nottingham.ac.uk, amalia.patane@nottingham.ac.uk and peter.beton@nottingham.ac.uk

Keywords: indium selenide, III–VI van der Waals layered crystals, 2D materials, physical vapour transport

Supplementary material for this article is available online

Abstract

We demonstrate that γ-InSe and the α, β and γ phases of In_2Se_3 can be grown epitaxially on ε-GaSe substrates using a physical vapour transport method. By exploiting the temperature gradient within the tube furnace, we can grow selectively different phases of In_xSe_y depending on the position of the substrate within the furnace. The uniform cleaved surface of ε-GaSe enables the epitaxial growth of the In_xSe_y layers, which are aligned over large areas. The In_xSe_y epilayers are characterised using Raman, photoluminescence, x-ray photoelectron and electron dispersive x-ray spectroscopies. Each In_xSe_y phase and stoichiometry exhibits distinct optical and vibrational properties, providing a tuneable photoluminescence emission range from 1.3 eV to ~2 eV suitable for exploitation in electronics and optoelectronics.

Introduction

Multi-layer van der Waals (vdW) heterostructures have the potential to extend the range of functionalities of optoelectronic devices [1]. These artificial structures, which are prepared by mechanical exfoliation and stacking of the component crystalline layers, have physical properties of fundamental and technological interest [2]. However, this method is not easily scalable for large-area device fabrication. This drawback can be overcome by the direct growth of 2D layers using vdW epitaxy [3]. Since vdW crystals have no dangling bonds and weak inter-layer forces, they can be grown on a vdW crystal or other substrates (SiO_2, mica, quartz, etc) with low levels of in-plane strain and form clean, sharp interfaces even in highly lattice-mismatched heterostructures [4–6].

To date, epitaxial growth by chemical vapour deposition (CVD), physical vapor transport (PVT) or molecular beam epitaxy (MBE) has been used for the synthesis of hexagonal boron nitride (hBN) [7–10], graphene [11–13], metal dichalcogenides [14–21] and metal chalcogenides [22–29]. Within this large family of vdW crystals, the epitaxial growth of metal chalcogenides containing In and Se, e.g. In_xSe_y, is now attracting increasing interest. These crystals can exist in different polytype phases, e.g. α, β, γ, and/or stoichiometries, i.e. different In/Se atomic ratio [30], each with a band structure that is strongly dependent on the number of atomic layers when the layer thickness is reduce below ~20 nm [31, 32]. Studies of exfoliated γ-InSe flakes have revealed properties that are distinct from those of other vdW crystals [33–35]. They are optically active with a band gap that increases markedly with decreasing layer thickness down to a single layer [33, 35]. In addition, the hybridization of the In and Se atomic orbitals leads to electron effective masses in the layer plane that are relatively small [34], giving rise to a high electron mobility at room temperature (>0.1 $m^2\ V^{-1}\ s^{-1}$) and at liquid-helium temperature (>1 $m^2\ V^{-1}\ s^{-1}$) [35], considerably higher than for the transition metal dichalcogenides [36].

Although advances have been achieved using mechanically exfoliated films of two-dimensional (2D) In_xSe_y with different polytypes and stoichiometries, the scalable synthesis of layers and heterostructures is still in its infancy. Growth by CVD and PVT has been explored only recently, with some success in producing specific polytypes of In_2Se_3 [22–24, 26, 27]. Different phases of InSe have also been produced by various techniques, such as pulsed laser deposition [37], atomic layer deposition (ALD) [38] and

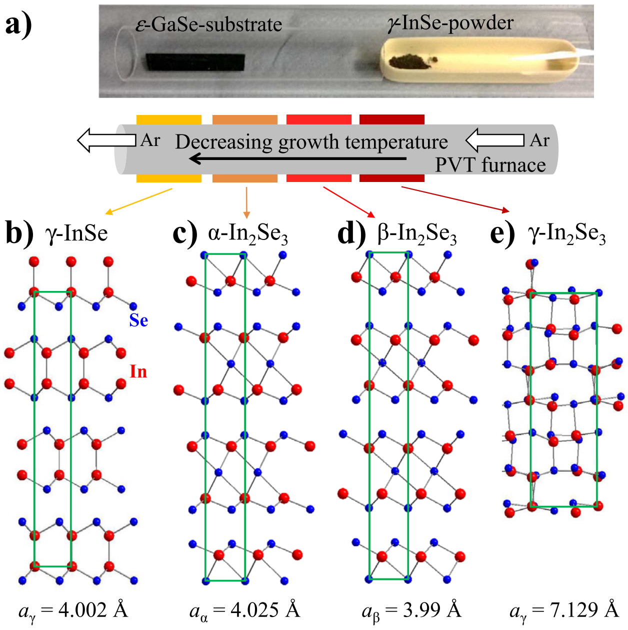

Figure 1. (a) Image and schematic diagram of the quartz tube for the PVT growth of In_xSe_y on ε-GaSe. The temperature gradient in the quartz tube enables the growth of different phases of In_xSe_y. (b)—(e) Side view of the crystal lattice and unit cell of γ-InSe (b), α-In_2Se_3 (c), β-In_2Se_3 (d) and γ-In_2Se_3 (e). The in-plane lattice constants are also shown for each phase. γ-InSe has rhombohedral crystal structure and the primitive unit cell contains three layers, each consisting of four closely-packed, covalently bonded, atomic sheets in the sequence Se–In–In–Se [33]. The α-In_2Se_3 and β-In_2Se_3 phases have the same rhombohedral crystal structure and the primitive unit cell contains three layers, each consisting of five covalently bonded, monoatomic sheets in the sequence Se–In–Se–In–Se. For α-In_2Se_3 the outer Se-atoms in each vdW layer are aligned, whereas in β-In_2Se_3 they are located into the interstitial sites of the Se-atoms in the neighbouring layers [41]. The γ-In_2Se_3 phase has hexagonal crystal structure with distorted wurtzite-type-like atomic arrangement [51].

MBE [39, 40]. Although these results are encouraging, the stoichiometry and polytype phase grown on specific substrates are generally difficult to predict and control; furthermore, different polytypes can coexist within the same structure. Addressing these challenges represents an important step towards the scalable production of high-quality materials and functional devices, thus overcoming the reliance on exfoliated crystals.

Here, we demonstrate the epitaxial growth by PVT on ε-GaSe substrates of large-area ($>10^3$ μm^2) In_xSe_y layers with a stoichiometry and phase that can be controlled by the temperature within the PVT furnace, see figure 1. The cleaved surface of ε-GaSe with its low density of dangling bonds enables the growth of large-area crystals of γ-InSe, and α, β and γ phases of In_2Se_3, despite the large lattice mismatch (between 6% and 47%) with the ε-GaSe-substrate (in-plane lattice constant 3.755 Å). We show that high-quality epilayers with well-defined vibrational and optical properties can also be grown on thin exfoliated flakes of ε-GaSe transferred onto a supporting SiO_2/Si-substrate. In particular, the different polytypes which we have grown exhibit bright photoluminescence (PL) emissions at room temperature covering a wide range from 1.3 eV for γ-InSe to 2 eV for γ-In_2Se_3. The wide choice of potential energy band alignments between the In_xSe_y layers and also with respect to ε-GaSe substrate are well suited to exploitation in electronics and optoelectronics.

Results and discussion

The indium selenide layers reported here were grown on the cleaved surface of ε-GaSe crystals by PVT. Details of the growth procedure are provided in the methods section. The as-grown layers (figures 2(a) and 3) have very different morphologies compared to those grown on SiO_2/Si (figure 2(b)) [26] and have coverage over larger areas ($>10^3$ μm^2). The thinnest films that form on ε-GaSe have a measured thickness, $t \approx 4$ nm. Their regular triangular shape is strikingly distinct from our previous PVT-grown layers on SiO_2/Si substrates which were near-circular, slightly facetted films (figure 2(b)) with lateral size of up to ~15×15 μm^2 and layer thickness down to 2.8 nm [26]. The AFM images in figures 2 and 3 suggest a common orientation and preferential alignment relative to the in-plane lattice vectors of the ε-GaSe hexagonal lattice. This is confirmed in the large area optical micrograph in figure 3(a) where the common alignment of triangular islands is clearly seen over a length scale ~100 μm; this implies that the lattice vectors of the grown layer and the substrate are either aligned, or misaligned by 30°; other misalignment angles would lead to multiple island orientations.

The chemical composition of the In_xSe_y layers grown on ε-GaSe was assessed by electron dispersive x-ray (EDX) and x-ray photoelectron spectroscopy (XPS). Analysis of the EDX (figure 3(d) and supporting information S1 (stacks.iop.org/TDM/5/035026/mmedia))

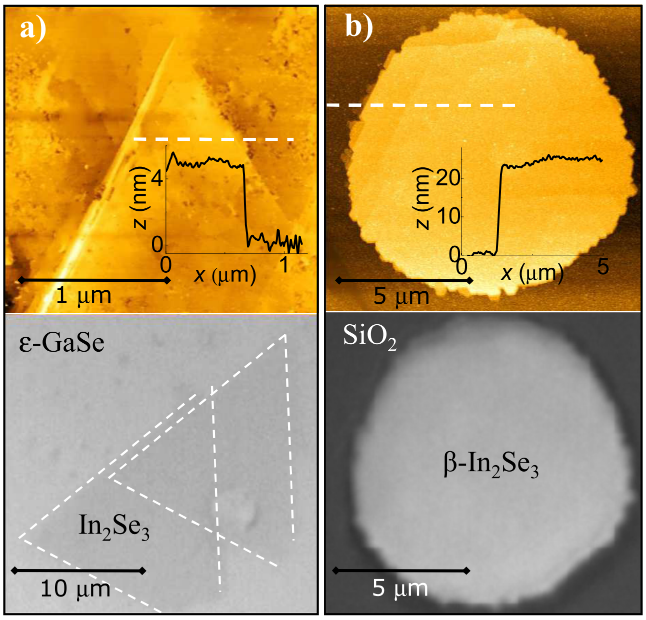

Figure 2. (a) and (b) Topographic AFM image and z-profile (top), and optical micrographs (bottom) of In_2Se_3 layers grown on (a) the cleaved surface of a bulk ε-GaSe substrate and (b) a SiO_2/Si substrate. The AFM z-profiles were obtained along the dashed lines shown in the AFM images.

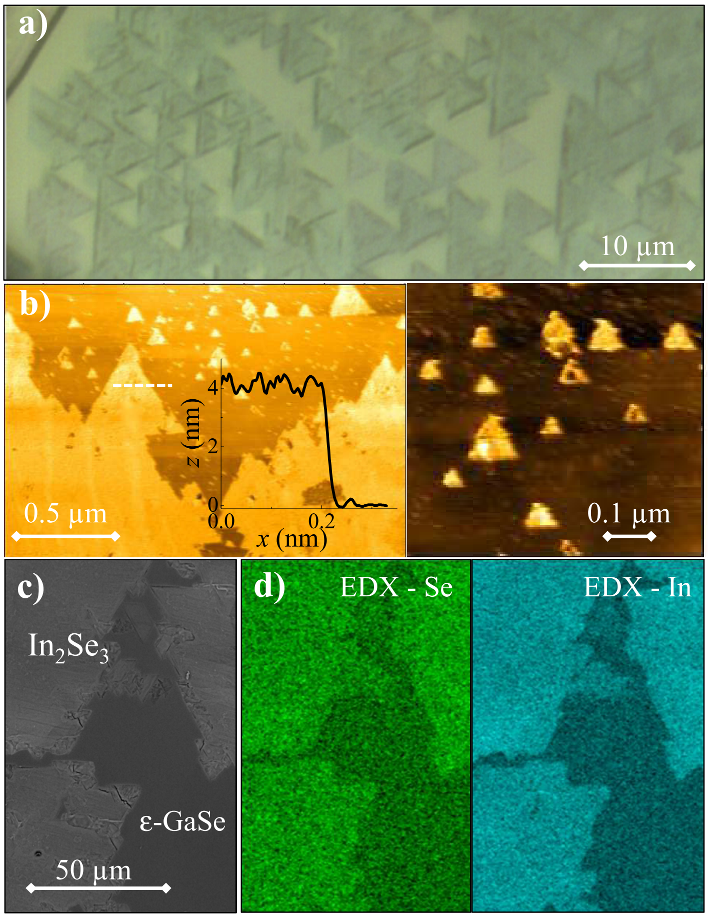

Figure 3. (a) Optical micrograph, (b) topographic AFM images and z-profile, (c) backscattered electron SEM image and (d) EDX elemental maps of In_2Se_3 grown on the cleaved surface of a bulk ε-GaSe substrate. The AFM z-profile was obtained along the dashed line shown in the AFM image.

and XPS spectra (supporting information S2) reveal a stoichiometric composition [In]:[Se] = 2:3, consistent with the formation of In_2Se_3. Identifying the specific crystalline phase of the In_2Se_3 layers is generally difficult: different phases (α, β, γ, δ, and κ) may co-exist and some may share similar properties [30].

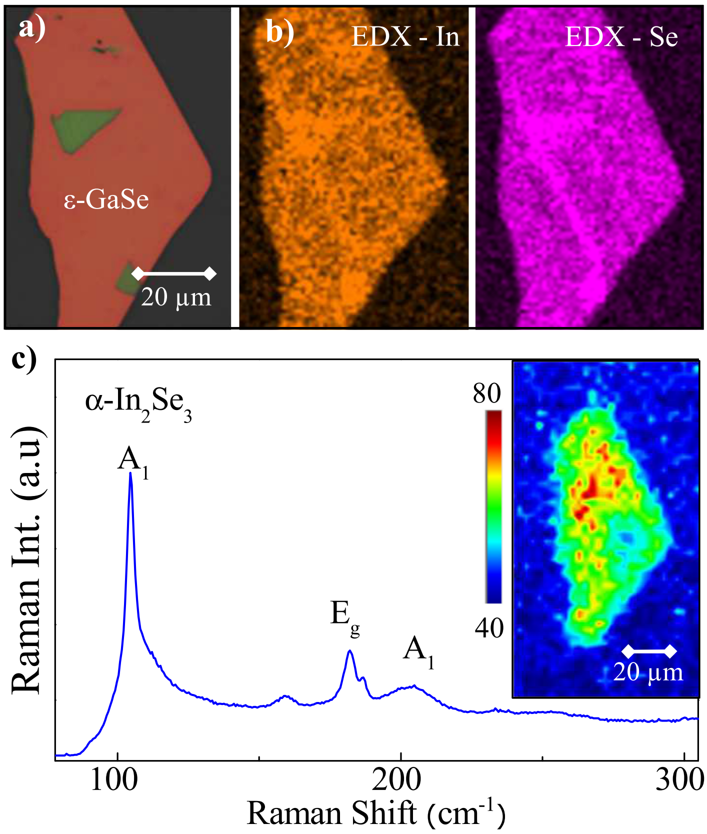

Figure 4. (a) Optical micrograph of an exfoliated ε-GaSe flake on a SiO_2/Si substrate before the growth. (b) EDX elemental maps and (c) Raman spectrum and map for α-In_2Se_3 grown on the exfoliated ε-GaSe flake shown in part (a). The Raman map was obtained by plotting the micro-Raman intensity at 105 cm^{-1} corresponding to the main A_1-mode of α-In_2Se_3 ($\lambda = 633$ nm and $P = 0.1$ mW).

In particular, whereas the crystal structures of γ- and δ-In_2Se_3 are hexagonal and trigonal respectively, the rhombohedral crystal structures of α- and β-In_2Se_3 phases are very similar to each other [41].

In general, Raman spectroscopy can help identify the crystalline phase of In_2Se_3 due to the presence of distinct vibrational modes for the different phases [41, 42]. However, in our case, due to the high background optical signal from the bulk ε-GaSe substrate (thickness ~1 mm), we were unable to detect distinct Raman modes from the thin In_2Se_3 layers. In order to identify different crystalline phases, we have adopted a different approach to growth and have investigated the growth on thin ε-GaSe exfoliated flakes (thickness ranging from 10 nm to 200 nm) on a SiO_2/Si substrate. The Raman background signal from these substrates is sufficiently weak (see below) to identify the phases of the grown In_xSe_y materials.

Figure 4(a) shows images of the growth of In_xSe_y on an ε-GaSe flake. Interestingly, we find that growth occurs exclusively on the ε-GaSe flakes with no deposition on the surrounding exposed SiO_2/Si substrate (figure 4(a)). Figure 4(b) shows EDX elemental maps of indium selenide layers grown on an exfoliated ε-GaSe flake at a substrate temperature, $T_s = 560$ °C ± 10 °C. The EDX analysis for this flake confirmed that the stoichiometric composition of the grown layers is In_2Se_3 (see supporting information S3). A typical room temperature ($T = 300$ K) micro-Raman spectrum of the In_2Se_3 layers is shown in figure 4(c). The Raman modes are centred at ~105, 159, 182, 187 and 203 cm^{-1} corresponding to the A_1-modes (105, 159, 182 and 203 cm^{-1}) and E_g-mode (187 cm^{-1}) of α-In_2Se_3 [43]. A colour plot of the intensity of the Raman peaks observed in this α-In_2Se_3 layer (inset of figure 4(c)) indicates that the α-phase does not coexist with other crystalline phases of In_2Se_3. In contrast, for the case of In_2Se_3 layers grown on a SiO_2/Si substrate at a similar substrate position and temperature in the furnace during previous growth runs [26], we find that the Raman peaks are centred at ~110, 175, and 205 cm^{-1}, corresponding to the intralayer vibrational A_1-modes (110 and 205 cm^{-1}) and the E_g-mode (175 cm^{-1}) of β-In_2Se_3 [26, 27].

Due to the temperature gradient within the tube furnace, we can grow different phases and stoichiometries of indium selenide during a single growth run depending on the position of each substrate within the quartz tube (figure 1). We have grown four different types of indium selenide in this way including the layered phases γ-InSe, α-In_2Se_3, β-In_2Se_3, and also γ-In_2Se_3 which has a 3D crystal structure (see figure 1(e)). In common with figure 4, for all of these phases we observe that growth occurs exclusively on the ε-GaSe flakes and no material is deposited on the exposed SiO_2 surface. The four different indium

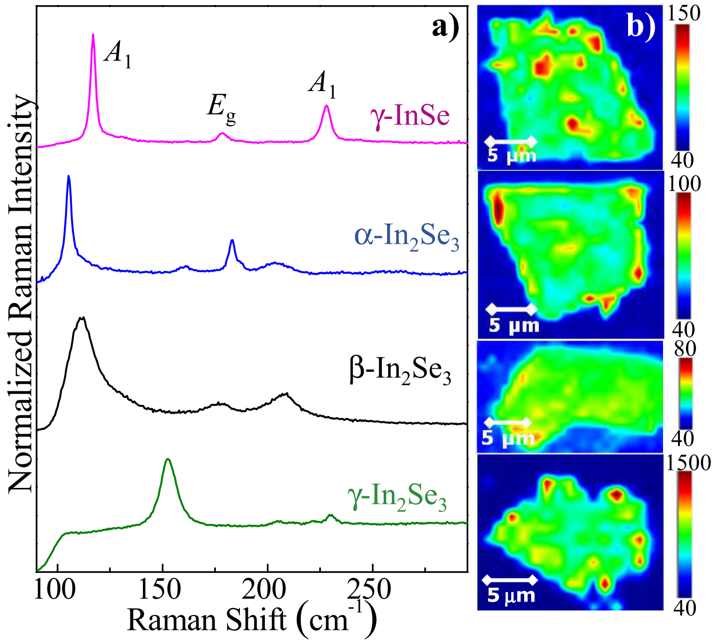

Figure 5. (a) Room temperature ($T = 300$ K) Raman spectra and (b) maps for In_xSe_y layers grown on exfoliated ε-GaSe flakes. The Raman maps were obtained by plotting the Raman intensity of the main A_1-mode in each In_xSe_y layer ($\lambda = 633$ nm and $P = 0.1$ mW).

selenide phases were grown on exfoliated flakes of ε-GaSe at different substrate temperatures, T_s, ranging between 500 °C and 580 °C (corresponding to 15 cm to 4 cm from the source material in our PVT furnace). The appearance of these phases in the observed sequence of decreasing temperatures is well matched with the temperature range over which they have been predicted to be stable in the phase diagram for the growth of In_xSe_y reported in [30].

Our as-grown In_xSe_y layers are chemically stable and optically active in air at room temperature over periods of several months. Distinct Raman modes are identified for the different phases of In_xSe_y (figure 5(a)). The Raman maps in figure 5(b) confirm that each crystalline phase is pure, with no mixing of phases. For γ-InSe, the Raman peaks are centred at ~117, 179, and 228 cm^{-1}, corresponding to the intralayer vibrational A_1-modes (117 and 228 cm^{-1}) and the E_g-mode (179 cm^{-1}), previously identified in [33]. The Raman modes of α-In_2Se_3 and β-In_2Se_3 phases are described earlier in this section. For γ-In_2Se_3 layers, the Raman peaks are centred at 152, 205, 221 and 230 cm^{-1} and agree well with previously reported values for bulk γ-In_2Se_3 [42, 44]. The full width at half maximum (FWHM) of the main Raman mode in γ-InSe (FWHM ≈ 3 cm^{-1}), α-In_2Se_3 (FWHM ≈ 4 cm^{-1}) and γ-In_2Se_3 (FWHM ≈ 9 cm^{-1}) are significantly narrower than for β-In_2Se_3 (FWHM ≈ 16 cm^{-1}), see figure 5(a).

Whereas the growth by PVT of 2D indium selenide layers has been demonstrated only recently for α-In_2Se_3 [22, 24] and β-In_2Se_3 [26, 27], the epitaxial growth of γ-InSe and γ-In_2Se_3 has proven more difficult to achieve. There have been recent reports of the growth of γ-InSe, a material of particular interest due to its attractive optical and electrical properties, using pulsed layer deposition (PLD) and ALD. A comparison of our results shows similar Raman peak positions and widths for material grown by PLD [37] and the results shown here; however, the Raman peaks for the material grown by ALD [38] are much broader and their position is closer to that expected for β-In_2Se_3 [27].

The room temperature ($T = 300$ K) and low temperature ($T = 10$ K) normalized PL spectra of as-grown γ-InSe, α-In_2Se_3, β-In_2Se_3 and γ-In_2Se_3 layers with thickness $t > 20$ nm are compared in figure 6(a). For γ-InSe, the room temperature PL emission is centred at an energy $E = 1.26$ eV and has a FWHM of ~80 meV, similar to that measured previously for our bulk crystals grown by the Bridgman-method [33, 45]. Similarly, the room temperature PL emission of as-grown α-In_2Se_3 has a peak at $E = 1.41$ eV, as measured for our bulk Bridgman-grown crystals. The PL emission of α-In_2Se_3 is narrower (FWHM ≈ 140 meV) and peaked at slightly lower energy than for as-grown β-In_2Se_3 ($E = 1.43$ eV and FWHM ≈ 170 meV). The room temperature PL spectrum of γ-In_2Se_3 is peaked at $E = 1.95$ eV and shows three much weaker bands at lower energies ($E = 1.44$ eV, 1.56 and 1.70 eV). We attribute the presence of these weaker bands to the recombination of carriers at localized states within the bandgap. For all the crystals, the low temperature ($T = 10$ K) PL emission peaks are centred at higher energies compared to those at $T = 300$ K, with the largest thermal shift (~200 meV) observed in γ-In_2Se_3. The energy shift is accompanied by a monotonic increase of the PL intensity by up to

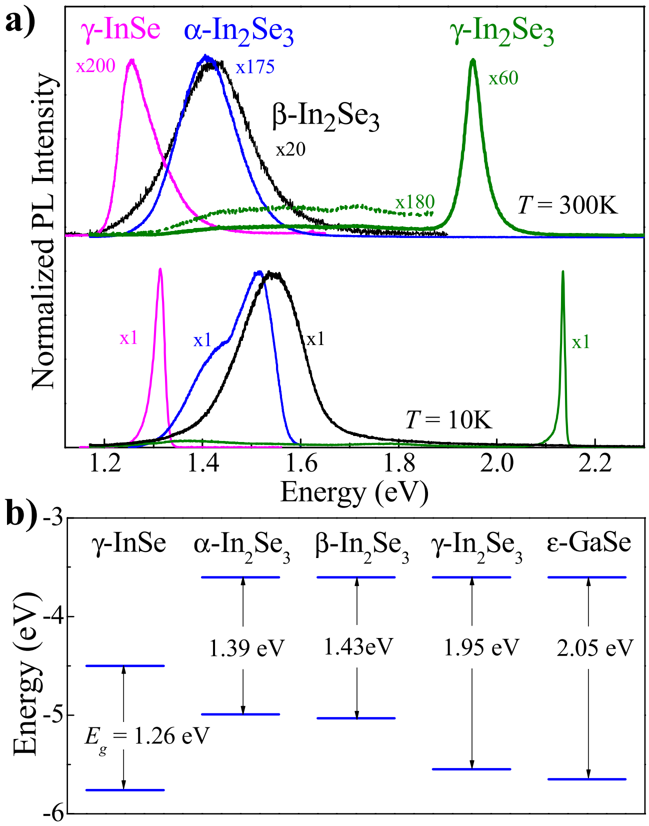

Figure 6. (a) Room temperature ($T = 300$ K) and low temperature ($T = 10$ K) μPL spectra of γ-InSe, α-In_2Se_3, β-In_2Se_3 and γ-In_2Se_3 layers grown on exfoliated ε-GaSe flakes. All optical measurements were conducted on films with thickness $t > 20$ nm. Layers of thickness $t < 20$ nm are required to observe a measurable increase of the direct band gap with decreasing t. (b) Schematic showing the band alignments [47, 48] of the materials which can be grown on ε-GaSe; the bandgaps of the different phases of In_xSe_y which we have grown are very close to the literature values.

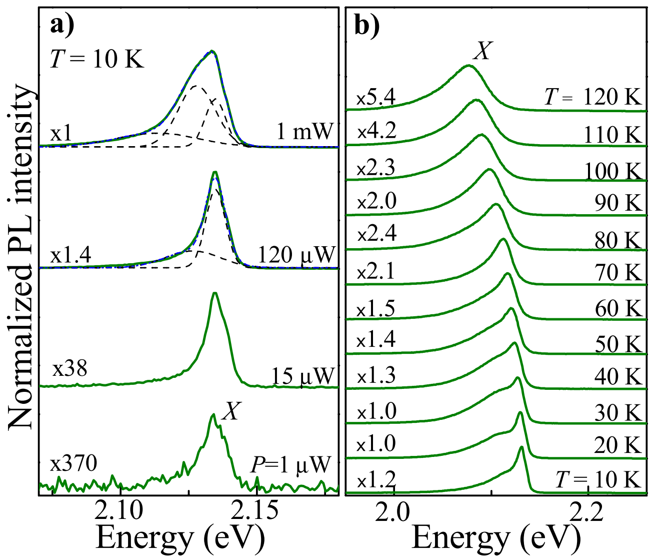

Figure 7. μPL spectra of γ-In_2Se_3 layers grown on exfoliated ε-GaSe flakes for (a) different excitation laser powers P ($T = 10$ K, $\lambda = 532$ nm) and (b) different temperatures ($\lambda = 532$ nm and $P = 3$ mW). The dashed-curves in (a) are the multi-peak Gaussian fits to the data.

a factor 200 when the temperature is decreased from 300 K to 10 K. These PL results confirm that our epitaxially grown layered phases are comparable in quality to bulk crystals grown by the Bridgman-method [33, 45] and material grown by PLD [37] highlighting the promise of this approach to growing metal chalcogenides.

The electronic and vibrational properties of the as-grown In_xSe_y layers can be influenced by the presence of crystal defects, such as In- and Se-vacancies

[30]. Vacancies can modify atomic orbitals and band gap energies due to ordering and bond relaxation [46]. These defects can also influence the position and linewidth of the Raman and PL lines due to disorder, lattice distortion and phonon scattering around the defects. As shown in figure 5, the Raman modes for β-In_2Se_3 and γ-In_2Se_3 tend to be broader than for α-In_2Se_3 and γ-InSe, suggesting that the latter phases have better crystalline quality. In particular, the low temperature PL spectra of the β-In_2Se_3 layers reveal a dominant carrier recombination from defects and/or impurity levels that is weakly dependent on the layer thickness (supplementary information S4). This behaviour contrasts with that of the other phases (γ-InSe, α-In_2Se_3 and γ-In_2Se_3) where narrow PL emissions are observed at low temperature due to recombination of excitons and/or carriers localized on shallow impurities (figure 6). In particular, the narrow PL-line in γ-In_2Se_3 reveals a structured PL spectrum, see figure 7. The apparently 'anomalous' and asymmetric line-shape of the PL band can be modelled by fitting it to two ($P = 120$ μW) or three ($P = 1$ mW) Gaussian components, as shown in figure 7(a). The high-energy line (X) is attributed to excitonic emission: it persists in the spectrum even at low power densities (figure 7(a)) and at high temperatures (figure 7(b)). The lower-energy tail of the spectrum is significantly reduced with respect to the X-line as the power decreases and/or the temperature increases. This behaviour is consistent with a contribution to the spectrum from charged exciton and/or biexcitons with binding energies larger than 20 meV.

Finally, using the electron affinity for bulk In_xSe_y and ε-GaSe [47, 48] and the band gap energies deduced from the measured PL spectra at RT, we plot in figure 6(b) the band alignments for different stoichiometries and phases. It can be seen that heterostructures based on these materials could offer several potential advantages over to existing semiconductor heterojunctions by enabling a diverse range of component layers even when the lattice mismatch is large, tuneable optical response over an extended NIR-VIS wavelength range, and a range of interesting band alignments and potential profiles.

Conclusions

In summary, we have demonstrated that the uniform cleaved surface of the vdW crystal ε-GaSe can be used as a substrate for the epitaxial growth of large-area (>10^3 μm^2) In_xSe_y layers. We have successfully grown four well-defined crystalline phases of In_xSe_y. The In_xSe_y compounds have a larger unit cell than ε-GaSe with an in-plane lattice mismatch ranging between 6% and 47%. The successful growth of γ-InSe, α-In_2Se_3, β-In_2Se_3 and γ-In_2Se_3 on exfoliated ε-GaSe nanolayers offers the prospect for large-area device fabrication and junction devices that exploit the distinctive optical absorption and luminescent emission of the component layers. Due to the absence of dangling bonds, different vdW crystals can be grown one upon another without any restriction on the lattice mismatch, a major obstacle with traditional all-covalent multicomponent semiconductor structures where the presence of strain relaxation and crystalline defects can quench the room temperature PL. The optical spectra and the temperature dependence indicate distinct electronic properties for the different stoichiometric phases of indium selenide and demonstrate a wide spectral range of PL from the visible (γ-In_2Se_3) to the near-infrared (γ-InSe, β-In_2Se_3 and α-In_2Se_3). In addition to different combinations of bandgaps and band alignments, the In_xSe_y polytypes and ε-GaSe offer additional attractive features, including lightweight and compatibility with different substrates, well suited for a range of novel applications, including ferroelectricity in α-In_2Se_3 [49] and high-sensitivity broad-band In_xSe_y/ε-GaSe photodiodes [50].

Methods

Synthesis of In_xSe_y layers

For the growth of In_xSe_y layers by physical vapour transport, we used Bridgman-grown high-quality γ-polytype InSe crystals ground into powder and placed in a tube furnace. The tube furnace comprised a 45 cm long Carbolite furnace, 1 m long both open ended quartz tube (tube diameter, $d = 3.2$ cm), a rotary pump and an Ar flow controller. The InSe powder was heated from $T = 25$ °C to 600 °C at a rate of 3 °C min^{-1} and kept at 600 °C for 4 to 9 h. An Ar flow of 150 sccm was used to provide a pressure of 1.6 mbar and to transport the vapour for deposition on a substrate, placed downstream at 4–15 cm away from the source material, which provides a substrate temperature range between $T_s \approx 580$ °C to 500 °C. The system was then allowed to cool slowly to room temperature over a period of 10 h.

Chemical and topographic characterization

The XPS measurements were performed using a Kratos AXIS ULTRA with a monochromatic Al Kα x-ray source ($h\nu = 1486.6$ eV) operated at 10 mA emission current and 12 kV anode potential ($P = 120$ W), and the data processing was performed using CASAXPS version 2.3.17PR1.1 software with Kratos sensitivity factors (RSFs) to determine atomic % values from the peak areas. The electron collection spot size is ~700 × 300 μm^2. All XPS binding energies were calibrated with respect to the C 1s peak at a binding energy of 284.8 eV. The scanning electron microscopy (SEM) and energy-dispersive x-ray (EDX) analysis were performed at 20 kV in high vacuum (~10^{-6} mbar) with an FEI Quanta 650 ESEM equipped with an Oxford Instruments X-Max^N 150 EDX detector. The topography images were acquired by an Asylum Research MFP-3D atomic force microscope (AFM) in tapping mode under ambient conditions.

Optical studies

The experimental set-up for μPL and Raman measurements comprised a He–Ne laser ($\lambda = 633$ nm) and a frequency-doubled Nd:YVO_4 laser ($\lambda = 532$ nm), an XY linear positioning stage or a cold-finger cryostat, an optical confocal microscope system, a spectrometer with 150 and 1200 groves mm^{-1} gratings, equipped with a charge-coupled device and a liquid-nitrogen cooled (InGa)As array photodetector. For the room temperature studies, the laser beam was focused to a diameter $d \approx 1$ μm using a 100× objective and the μPL spectra were measured at low power ($P \sim 0.1$ mW) to avoid lattice heating. For the low T studies the laser beam (P up to 12 mW) was focused through the window of an optical cryostat to a diameter $d \approx 3$ μm using a 50× objective.

Acknowledgment

This work was supported by the Engineering and Physical Sciences Research Council (grant numbers EP/M012700/1 and EP/K005138/1) (EPSRC); the European Research Council (ERC) under the European Union's Horizon 2020 research and innovation programme (grant agreement number 696656); The University of Nottingham and the National Academy of Sciences of Ukraine.

Supplementary data

Supporting information available: EDX and XPS spectra of In_2Se_3 films grown on a bulk ε-GaSe substrate; EDX maps and spectrum of In_2Se_3 grown on an exfoliated ε-GaSe flake; and low temperature PL spectra of β-In_2Se_3 layers grown on a SiO_2/Si substrate. The data, including images and spectroscopic measurements, on which this manuscript was based is available as on online resource with digital object identifier https://doi.org/10.17639/nott.355.

ORCID iDs

Nilanthy Balakrishnan https://orcid.org/0000-0002-7236-5477
Amalia Patanè https://orcid.org/0000-0003-3015-9496
Peter H Beton https://orcid.org/0000-0002-2120-8033

References

[1] Ferrari A C *et al* 2015 Science and technology roadmap for graphene, related two-dimensional crystals, and hybrid systems *Nanoscale* **7** 4598–810
[2] Geim A K and Grigorieva I V 2013 van der Waals heterostructures *Nature* **499** 419–25
[3] Jaegermann W, Klein A and Pettenkofer C 2002 Electronic properties of van der Waals-epitaxy films and interfaces *Electron Spectroscopies Applied to Low-Dimensional Materials* ed H Hughes and H Starnberg (Dordrecht: Kluwer) pp 317–402
[4] Li M-Y *et al* 2015 Epitaxial growth of a monolayer WSe_2–MoS_2 lateral p-n junction with an atomically sharp interface *Science* **349** 254–528
[5] Sahoo P K *et al* 2018 One-pot growth of two-dimensional lateral heterostructures via sequential edge-epitaxy *Nature* **553** 63–7
[6] Li H, Shi Y and Li L J 2018 Synthesis and optoelectronic applications of graphene/transition metal dichalcogenides flat-pack assembly *Carbon* **127** 602–10
[7] Nakhaie S *et al* 2015 Synthesis of atomically thin hexagonal boron nitride films on nickel foils by molecular beam epitaxy *Appl. Phys. Lett.* **106** 213108
[8] Liu Z *et al* 2011 Direct growth of graphene/hexagonal boron nitride stacked layers *Nano Lett.* **11** 2032–7
[9] Cho Y-J *et al* 2016 Hexagonal boron nitride tunnel barriers grown on graphite by high temperature molecular beam epitaxy *Sci. Rep.* **6** 34474
[10] Zuo Z *et al* 2015 *In situ* epitaxial growth of graphene/h-BN van der Waals heterostructures by molecular beam epitaxy *Sci. Rep.* **5** 14760
[11] Hwang J *et al* 2013 van der Waals epitaxial growth of graphene on sapphire by chemical vapor deposition without a metal catalyst *ACS Nano* **7** 385–95
[12] Yang W *et al* 2013 Epitaxial growth of single-domain graphene on hexagonal boron nitride *Nat. Mater.* **12** 792–7
[13] Sun Z *et al* 2010 Growth of graphene from solid carbon sources *Nature* **468** 549–52
[14] Shi Y *et al* 2012 van der Waals epitaxy of MoS_2 layers using graphene as growth templates *Nano Lett.* **12** 2784–91
[15] Shim G W *et al* 2014 Large-area single-layer $MoSe_2$ and its van der Waals heterostructures *ACS Nano* **8** 6655–62
[16] Wang S, Wang X and Warner J H 2015 All chemical vapor deposition growth of MoS_2: h-BN vertical van der Waals heterostructures *ACS Nano* **9** 5246–54
[17] Okada M *et al* 2014 Direct chemical vapor deposition growth of WS_2 atomic layers on hexagonal boron nitride *ACS Nano* **8** 8273–7
[18] Choudhary N *et al* 2016 Centimeter scale patterned growth of vertically stacked few layer only 2D MoS_2/WS_2 van der Waals heterostructure *Sci. Rep.* **6** 25456
[19] Gong Y *et al* 2014 Vertical and in-plane heterostructures from WS_2/MoS_2 monolayers *Nat Mater.* **13** 1135–42
[20] Zhou X *et al* 2017 Vertical heterostructures based on $SnSe_2$/MoS_2 for high performance photodetectors *2D Mater.* **4** 25048
[21] Liang D, Schmidt J R and Jin S 2014 Vertical heterostructures of layered metal chalcogenides by van der Waals epitaxy *Nano Lett.* **14** 3047–54
[22] Lin M *et al* 2013 Controlled growth of atomically thin In_2Se_3 flakes by van der Waals epitaxy *J. Am. Chem. Soc.* **135** 13274–7
[23] Zheng W *et al* 2015 Patterning two-dimensional chalcogenide crystals of Bi_2Se_3 and In_2Se_3 and efficient photodetectors *Nat. Commun.* **6** 6972
[24] Zhou J *et al* 2015 Controlled synthesis of high-quality monolayered α-In_2Se_3 via physical vapor deposition *Nano Lett.* **15** 6400–5
[25] Li X *et al* 2015 van der Waals epitaxial growth of GaSe domains on graphene *ACS Nano* **9** 8078–88
[26] Balakrishnan N *et al* 2016 Quantum confinement in β-In_2Se_3 layers grown by physical vapour transport for high responsivity photodetectors *2D Mater.* **3** 25030
[27] Zhou S, Tao X and Gu Y 2016 Thickness-dependent thermal conductivity of suspended two-dimensional single-crystal In_2Se_3 layers grown by chemical vapor deposition *J. Phys. Chem.* C **120** 4753–8
[28] Ben Aziza Z *et al* 2016 van der Waals epitaxy of GaSe/graphene heterostructure: electronic and interfacial properties *ACS Nano* **10** 9679–86
[29] Chen M-W *et al* 2018 Large-grain MBE-grown GaSe on GaAs with a Mexican hat-like valence band dispersion *npj 2D Mater. Appl.* **2** 2

[30] Han G, Chen Z G, Drennan J and Zou J 2014 Indium selenides: structural characteristics, synthesis and their thermoelectric performances *Small* **10** 2747–65
[31] Rybkovskiy D V, Osadchy A and Obraztsova E D 2014 Transition from parabolic to ring-shaped valence band maximum in few-layer GaS, GaSe, and InSe *Phys. Rev.* B **90** 1–9
[32] Zólyomi V, Drummond N D and Fal'ko V I 2014 Electrons and phonons in single layers of hexagonal indium chalcogenides from *ab initio* calculations *Phys. Rev.* B **89** 205416
[33] Mudd G W *et al* 2013 Tuning the bandgap of exfoliated InSe nanosheets by quantum confinement *Adv. Mater.* **25** 5714–8
[34] Mudd G W *et al* 2016 The direct-to-indirect band gap crossover in two-dimensional van der Waals Indium Selenide crystals *Sci. Rep.* **6** 39619
[35] Bandurin D A *et al* 2017 High electron mobility, quantum Hall effect and anomalous optical response in atomically thin InSe *Nat. Nanotechnol.* **12** 223–7
[36] Choi W *et al* 2017 Recent development of two-dimensional transition metal dichalcogenides and their applications *Mater. Today* **20** 116–30
[37] Yang Z *et al* 2017 Wafer-scale synthesis of high-quality semiconducting two-dimensional layered InSe with broadband photoresponse *ACS Nano* **11** 4225–36
[38] Browning R, Kuperman N, Moon B and Solanki R 2017 Atomic layer growth of InSe and Sb_2Se_3 layered semiconductors and their heterostructure *Electronics* **6** 27
[39] Hayashi T, Ueno K, Saiki K and Koma A 2000 Investigation of the growth mechanism of an InSe epitaxial layer on a MoS_2 substrate *J. Cryst. Growth* **219** 115–22
[40] Sánchez-Royo J F *et al* 2001 Optical and photovoltaic properties of indium selenide thin films prepared by van der Waals epitaxy *J. Appl. Phys.* **90** 2818–23
[41] Ke F *et al* 2014 Interlayer-glide-driven isosymmetric phase transition in compressed In_2Se_3 *Appl. Phys. Lett.* **104** 1–2
[42] Weszka J *et al* 2000 Raman scattering in In_2Se_3 and $InSe_2$ amorphous films *J. Non. Cryst. Solids* **265** 98–104
[43] Lewandowska R, Bacewicz R, Filipowicz J and Paszkowicz W 2001 Raman scattering in alpha-In_2Se_3 crystals *Mater. Res. Bull.* **36** 2577–83
[44] Marsillac S, Combot-Marie A M, Bernède J C and Conan A 1996 Experimental evidence of the low-temperature formation of γ-In_2Se_3 thin films obtained by a solid-state reaction *Thin Solid Films* **288** 14–20
[45] Balakrishnan N *et al* 2017 Engineering *p-n* junctions and bandgap tuning of InSe nanolayers by controlled oxidation *2D Mater.* **4** 25043
[46] Nakayama T and Ishikawa M 1997 Bonding and optical anisotropy of vacancy-ordered Ga_2Se_3 *J. Phys. Soc. Japan* **66** 3887–92
[47] Lang O *et al* 1999 Thin film growth and band lineup of In_2O_3 on the layered semiconductor InSe *J. Appl. Phys.* **86** 5687–91
[48] Drapak S I, Kovalyuk Z D, Netyaga V V and Orletski V B 2002 On the mechanisms of current transfer in n-In_2Se_3-p-GaSe heterostructures *Tech. Phys. Lett.* **28** 707–10
[49] Ding W *et al* 2017 Prediction of intrinsic two-dimensional ferroelectrics in In_2Se_3 and other III_2–VI_3 van der Waals materials *Nat. Commun.* **8** 14956
[50] Yan F *et al* 2017 Fast, multicolor photodetection with graphene-contacted p-GaSe/n-InSe van der Waals heterostructures *Nanotechnology* **28** 27LT01
[51] Pfitzner A and Lutz H D 1996 Redetermination of the crystal structure of γ-$In_2Se_3$by twin crystal x-ray method *J. Solid State Chem.* **124** 305–8